Japanese Journal of Applied Physics **55**, 07KF12 (2016)
http://doi.org/10.7567/JJAP.55.07KF12

REGULAR PAPER

Estimation of size of red blood cell aggregates using backscattering property of high-frequency ultrasound: In vivo evaluation

Yusaku Kurokawa[1], Hirofumi Taki[1,2*], Satoshi Yashiro[3], Kan Nagasawa[3], Yasushi Ishigaki[3], and Hiroshi Kanai[1,2*]

[1]*Graduate School of Biomedical Engineering, Tohoku University, Sendai 980-8579, Japan*
[2]*Graduate School of Engineering, Tohoku University, Sendai 980-8579, Japan*
[3]*The Department of Internal Medicine Division of Diabetes and Metabolism, Iwate Medical University, Morioka 020-8505, Japan*

*E-mail: taki@ecei.tohoku.ac.jp; kanai@ecei.tohoku.ac.jp

Received November 14, 2015; accepted March 18, 2016; published online June 16, 2016

We propose a method for assessment of the degree of red blood cell (RBC) aggregation using the backscattering property of high-frequency ultrasound. In this method, the scattering property of RBCs is extracted from the power spectrum of RBC echoes normalized by that from the posterior wall of a vein. In an experimental study using a phantom, employing the proposed method, the sizes of microspheres 5 and 20 μm in diameter were estimated to have mean values of 4.7 and 17.3 μm and standard deviations of 1.9 and 1.4 μm, respectively. In an in vivo experimental study, we compared the results between three healthy subjects and four diabetic patients. The average estimated scatterer diameters in healthy subjects at rest and during avascularization were 7 and 28 μm, respectively. In contrast, those in diabetic patients receiving both antithrombotic therapy and insulin therapy were 11 and 46 μm, respectively. These results show that the proposed method has high potential for clinical application to assess RBC aggregation, which may be related to the progress of diabetes.

1. Introduction

Medical ultrasound is widely and repetitively used for diagnosis[1–5] and treatment[6–8] in clinical settings because it is noninvasive and easy to use. For the diagnosis of atherosclerosis, ultrasound imaging is used to observe morphological changes in the arterial wall. The condition of blood is also an important marker for the diagnosis of circulatory diseases such as atherosclerosis in the early stage;[9,10] however, noninvasive quantitative estimation of the condition of blood is still challenging.

Red blood cells (RBCs) are the principal components of blood, and several researchers have focused on the characteristics of the echo returned from RBCs.[11,12] RBC aggregation is one of the primary determinants of blood viscosity,[9,13] and it increases microvascular flow resistance because of the additional energy required for disaggregation at the beginning of microcirculation.[14] Since excessive RBC aggregation should impair microcirculation flow, it may aggravate the microvascular complications resulting from metabolic disorder.[15] Furthermore, RBC aggregation deteriorates in subjects with diabetes, resulting from glycation of the surface membrane protein in hemoglobin.[16] In addition, excessive RBC aggregation depresses shear stress on the vascular wall, and the depression of shear stress leads to endothelial dysfunction and a characteristic change in the smooth muscle of the vascular wall.[17,18] These phenomena increase the risk of thrombosis and atherosclerosis, and thus it is very important to noninvasively assess RBC aggregation.

In the field of ultrasound imaging, it is known that smokelike echoes occur during RBC aggregation.[19] However, the assessment of RBC aggregation from the smokelike echoes is qualitative. Therefore, it is necessary to evaluate RBC aggregation quantitatively. Sato et al. have reported a technique to estimate RBC aggregation using the ultrasonic peak frequency, which they investigated in a basic experimental study using a silicone tube.[20] Also, many papers have reported on the assessment of the condition of blood. Paeng and coworkers observed the variation of blood echogenicity during the cardiac cycle.[21,22] Calle and coworkers observed changes in the sound speed and scatterer size on blood coagulation by in vitro measurement.[23,24] Franceschini et al. estimated the size of RBC aggregates using the structure factor size and attenuation estimator.[25] However, such studies required invasive processes.

In our previous study,[26] we proposed a noninvasive quantitative method for the assessment of RBC aggregation using high-frequency ultrasound. RBC aggregation was estimated by fitting the measured power spectrum to one of the theoretical power spectra of several scatterer sizes. Before the fitting process, the power spectrum of RBC echoes was normalized by that of the posterior wall of the vein to extract the scattering property. The echoes from the posterior wall of the vein were measured in M-mode measurement. Therefore, the signal-to-noise ratio (SNR) of the power spectrum for the posterior wall of the vein was low because the RF echoes were measured at a single location on the posterior wall of the vein.

In the present study, we improved the measurement method and assessed its performance by in vivo experiment. The proposed method improved the SNR of the reference power spectrum by coherent integration and modification of the measurement conditions. In our previous study, the reference power spectrum from the posterior wall of a vein was calculated from a single echo. In contrast, the proposed method uses several echoes selected in B-mode measurement to improve the SNR. The RF echoes from RBCs were measured when the blood flow was stopped by avascularization to induce a blood condition leading to RBC aggregation. In our previous study, blood flow was stopped by applying pressure manually with a cuff. However, the time required for complete avascularization varied. Therefore, an avascularization system was prepared using an air compressor with a cuff to measure all subjects under the same measurement conditions. Furthermore, three healthy subjects and 26 diabetic patients were measured and the performance of the proposed method was assessed.

2. Materials and methods

2.1 Frequency characteristics of ultrasound backscattering from RBCs

The diameter of an RBC is about 8 μm, which is sufficiently

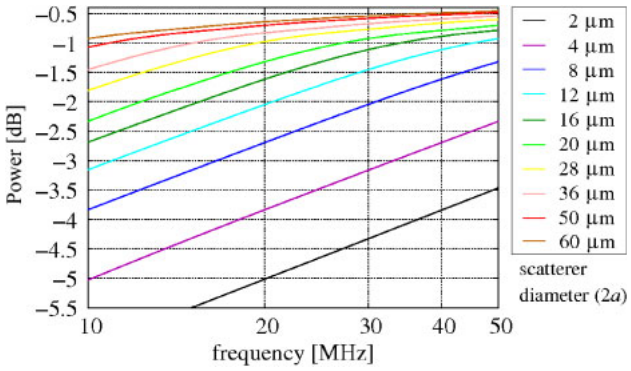

Fig. 1. (Color online) Theoretical power spectrum $\log_{10}[Q(ka)/4\pi a^2]$ for each scatterer diameter ($2a$).

small compared with the ultrasonic wavelength of 40 μm at a frequency of 40 MHz. When the scatterer size is much smaller than the transmission wavelength, the frequency spectrum of the echo from the scatterer follows Rayleigh's scattering law, where its power spectrum is proportional to the fourth power of the frequency. In contrast, when the size of a scatterer is large, the scatterer is regarded as a reflector and the power spectrum does not show frequency dependence. In this study, a scatterer was modeled by assuming an infinite number of infinitesimal point sources on the surface of a spherical scatterer.[27] When a plane wave is irradiated to the scatterer, the theoretical power spectrum $Q(ka)/4\pi a^2$ of the scattered echo is given by[28]

$$\frac{Q(ka)}{4\pi a^2} = \sum_{n=0}^{\infty} \frac{2n+1}{(ka)^2} \sin^2[\delta'_n(ka)], \tag{1}$$

where $Q(ka)$ is the scattering cross section, k is the wave number, a is the radius of the scatterer, n is the number of point sources on the surface of the scatterer, and $\delta'_n(ka)$ is the derivative of the phase difference between the incident wave and the scattered wave. The theoretical power spectrum $Q(ka)/4\pi a^2$ is given as a function of frequency f and scatterer radius a (a ranges from 1 to 30 μm) by transforming ka into $2\pi(a/\lambda) = (2\pi/c)fa$, where c is the acoustic velocity. Figure 1 shows the theoretical power spectrum for each scatterer diameter $2a$.

2.2 Normalization of power spectrum

The measured power spectrum $P_s(f)$ of the echoes from RBCs of the dorsal hand vein depends not only on the scattering properties of the scatterers, $S(f)$, but also on three other factors: the frequency response of the transmitting and receiving transducers, $G(f)$, the attenuation property of the propagation medium, $A_1(f)$, and the frequency spectrum caused by the voltage applied to the transducer, $X(f)$. In this study, the scattering properties of the aggregated RBCs were extracted by normalization using the power spectrum $P_r(f)$ of a flat vein wall. This process is expressed by[18]

$$10\log_{10}\frac{P_s(f)}{P_r(f)} = 10\log_{10}\frac{|S(f)G(f)A_1(f)X(f)|^2}{|R(f)G(f)A_2(f)X(f)|^2} \approx 10\log_{10}\frac{|S(f)|^2}{|R(f)|^2}, \tag{2}$$

where $R(f)$ is the reflection property of the venous wall and $A_2(f)$ is the attenuation property of the propagation medium for the measurement of the venous wall. In the present study, $A_2(f)$ is assumed to be the same as $A_1(f)$. We assume that $R(f)$ is equal to a positive constant R_0, that is, the reflection property does not have frequency dependence because the venous wall is assumed to be a flat reflector. Therefore, Eq. (2) can be rewritten as

$$10\log_{10}\frac{P_s(f)}{P_r(f)} \approx 10\log_{10}\frac{|S(f)|^2}{|R_0|^2}. \tag{3}$$

Therefore, the scattering properties of the scatterers, $S(f)$, can be obtained by this normalization process, that is, $P_s(f)$ is divided by $P_r(f)$.

2.3 Calculation of reference power spectrum

In the proposed method, the reference power spectrum $P_r(f)$ for in vivo measurement is calculated from the echoes from the lumen–intima interface of the posterior venous wall. The echoes from a lumen–intima interface are sometimes unclear, and some of them are similar to the echo from a media–adventitia interface. Since the reference power spectrum $P_r(f)$ should be estimated from the echo that returned from a single flat interface, the above-mentioned cases should be excluded.

In the present study, therefore, two processes were used: one was the selection of ultrasonic echoes from a lumen–intima interface located far from the echoes from a media–adventitia interface, and the other was the improvement of SNR by coherent integration. In the echo selection process, the ratio of the power of a center region to a tail region of the RF echo is calculated and echoes with a high ratio are selected. Figure 2 shows the RF echoes from a lumen–intima interface and their frequency spectra. The width of the window function was equal to double the pulse width of the ultrasound diagnostic equipment to extract the echo from the lumen–intima interface. When the extracted signal includes only the RF echoes from a lumen–intima interface, as shown in Fig. 2(a), no dip in the power spectrum appears around the center frequency, as shown in Fig. 2(b). However, when a media–adventitia interface is close to a lumen–intima interface, the signal extracted by the window function includes part of the echo from the media–adventitia interface in the tail region, as shown in Fig. 2(c), resulting in a small dip at a frequency of about 25 MHz in the power spectrum as shown in Fig. 2(d).

In the coherent integration process, we calculate the ratio of the power of a center region to that of a tail region for each ultrasound beam, and we choose the RF echo with a maximum ratio as the reference echo. From the cross-correlation between the reference echo and each of the other RF echoes around the lumen–intima interface of other beams, its time shift is determined. Each RF echo is shifted and averaged, and the power spectrum is obtained.

2.4 Estimation of RBC aggregate size

We estimate the size of an RBC aggregate by fitting the measured RBC echo after the normalization process to the theoretical echo based on Rayleigh scattering, where the difference between the measured frequency spectrum $10\log_{10}[P_s(f)/P_r(f)]$ of Eq. (3) and the theoretical frequency spectrum $10\log_{10}[Q(ka)/4\pi a^2]$ of Eq. (1) is minimized.[18] The minimization process is expressed by

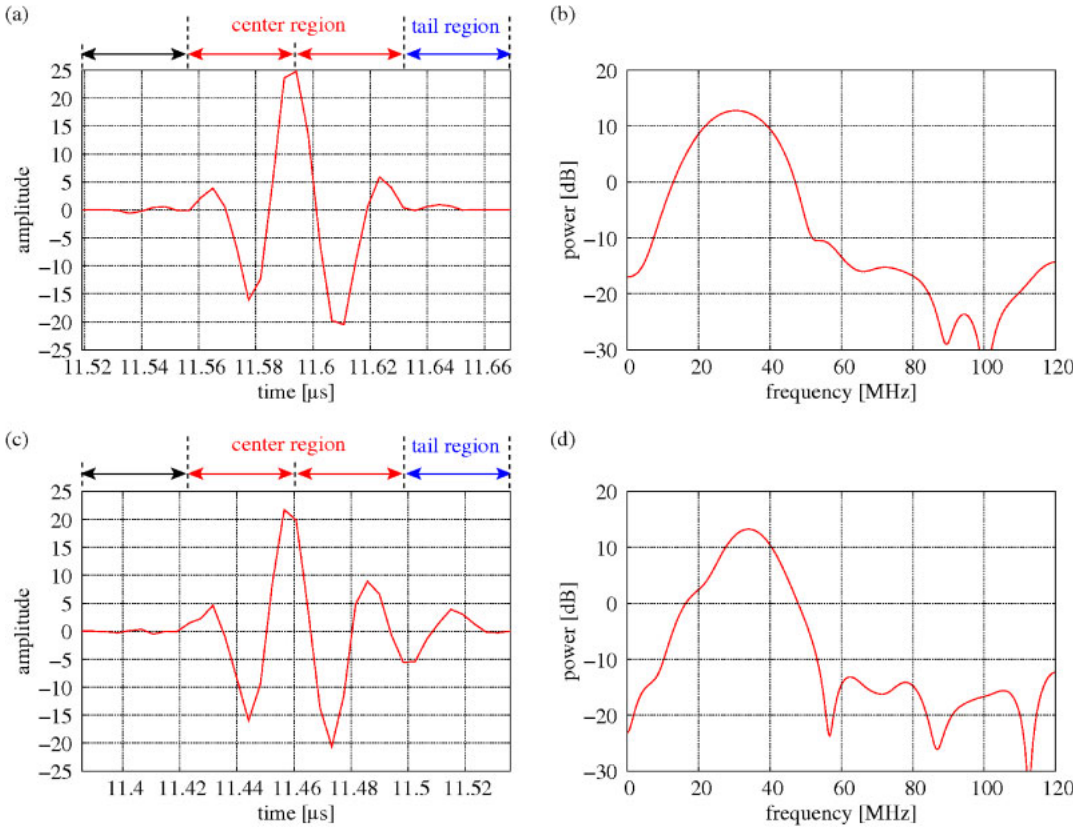

Fig. 2. (Color online) (a) RF echo from lumen–intima interface. (b) Frequency spectrum of RF echo from lumen–intima interface. (c) RF echo from lumen–intima interface and media–adventitia interface. (d) Frequency spectrum of RF echo from lumen–intima interface and media–adventitia interface.

$$\min_{a,b} \varepsilon(a,b) = \min_{a,b} \frac{1}{N} \sum_{k=0}^{N-1} w(f_k)[y(f_k) - \hat{y}(f_k, 2a, b)]^2, \quad (4)$$

where $y(f_k) = 10\log_{10}[P_s(f)/P_r(f)]$, $\hat{y}(f_k, 2a, b) = 10\log_{10}[bQ(ka)/4\pi a^2]$, f_k is the kth frequency, and $w(f_k)$ is the weighting function.

In this study, the weighting function $w(f_k)$ was selected to emphasize the frequency component with high SNR. Since the power spectrum $P_s(f)$ of the scattered echoes contains noise components, the noise spectrum is compensated by using the power spectrum $P_{noise}(f)$ of RF echoes from the water by

$$w(f_k) = P_s(f) - P_{noise}(f). \quad (5)$$

Figure 3 shows the measured frequency spectrum after normalization (red line), the weighting function $w(f_k)$ (blue line), and the theoretical frequency spectrum (green line) for the estimated scatterer size of 12 μm. We prepared the theoretical frequency spectrum for each of the scatterer diameters $2a$ from 2 to 60 μm, that is, the scatterer radii $a = 1, 2, 3, \ldots, 30$ μm. RBC aggregation was estimated by fitting the measured power spectrum to each of the prepared theoretical power spectra. The estimated scatterer size was limited from 2 to 60 μm.

2.5 Basic experiments using microspheres

Ultrasound diagnostic equipment (Tomey UD-8000) with a mechanical scan probe having a center frequency of 40 MHz and a focal length of 9 mm was used. The RF echoes were acquired at a sampling frequency of 240 MHz, and their power spectra were obtained by applying the Fourier transform with a Hanning window of 0.15 μs (36 points) in length.

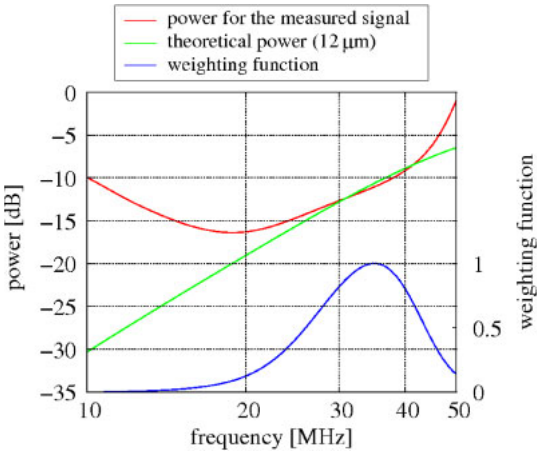

Fig. 3. (Color online) Measured normalized power spectrum $\log_{10}[P_s(f)/P_r(f)]$, theoretical power spectrum $\log_{10}[Q(ka)/4\pi a^2]$, and weighting function $w(f_k)$.

Microspheres (Dantec Dynamics Polyamide Seeding Particles) with diameters of 5, 20, and 50 μm were used. The microsphere density was 2.0 g/l for the microspheres with diameters of 5 and 20 μm. In contrast, it was 20.0 g/l for the microspheres of 50 μm diameter because the number of microspheres was not sufficient at a density of 2.0 g/l. To disperse the microspheres, polyoxyethylene octylphenyl ether was used as the surfactant. The measurement was repeated 15 times, where the fluid was stirred during each measurement. Therefore, the scatterer size was estimated 15 times for each

microsphere size. To eliminate the blocking effect of microspheres on the RF echo from a silicone plate, we measured the echo from the silicone plate located in water without microspheres.

2.6 In vivo experiments

RBC aggregation occurs when the blood shear rate is low.[14,29,30] Therefore, we measured ultrasonic echoes from RBCs with and without blood flow, the blood flow being stopped by the application of pressure of about 250 mmHg using a cuff on the upper arm.

The measurement procedure was as follows. First, the posterior wall of the vein was set at the focus of the US device, and RF echoes from a lumen–intima interface were acquired. Then, the lumen of the vein was set at the focus, and RF echoes from the RBCs were acquired while the subject was at rest for 1 min and during avascularization for 2 min. The power spectrum $P_s(f)$ of the echoes from RBCs was calculated by averaging 339 power spectra of RF echoes, three echoes from each of the 113 scan lines being extracted. The difference in RBC aggregation between at rest and during avascularization was evaluated. In this study, we created an avascularization system using an air compressor and a cuff to measure several subjects under the same conditions.

We applied this method to three healthy subjects and 26 diabetic patients including four patients receiving both antithrombotic therapy and insulin therapy in the clinical study. Each healthy subject was measured three times on different days. Each diabetic patient was measured once.

This research was approved by the Ethics Committee for Clinical Research at Graduate School of Engineering, Tohoku University, and that at Iwate Medical University. Measurements were conducted only after obtaining written informed consent following an explanation of the study content to the subjects.

3. Results

3.1 Basic experiments using microspheres

Figure 4 shows the average power spectra of the microsphere echoes and that of the echoes from the silicone plate. The microsphere size was estimated by fitting the measured power spectrum to each of the theoretical power spectra for the 30 scatterer sizes.

As shown in Fig. 4(a), the power spectrum of the 50 µm echo has a dip at a frequency of about 25 MHz. This might have originated from the resonance of 50 µm microspheres. The dip in the power spectrum caused a negative slope with respect to frequency after normalization. Since the theoretical power spectrum has a positive slope, the proposed method failed to estimate the size of the 50 µm microspheres. Therefore, we estimated the sizes of the 5 and 20 µm microspheres using the proposed method as follows.

Figure 5 shows the measured power spectra after normalization using the reference power spectrum from the silicone plate shown in Fig. 4(b), the theoretical power spectra for the estimated scatterer diameters, and the weighting function. In this measurement, the diameters of the 5 and 20 µm microspheres were estimated to be 6 and 18 µm, respectively. Each measured power spectrum is close to the theoretical one in the frequency band from 30 to 50 MHz, where each weighting function has a large value.

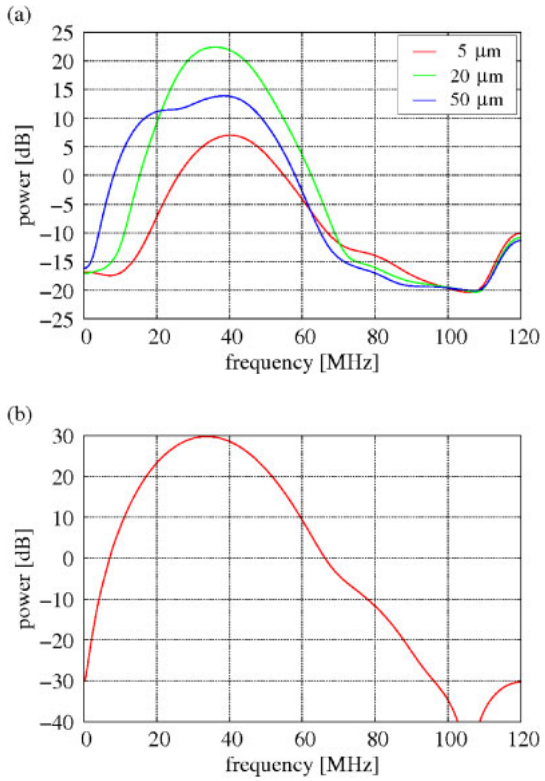

Fig. 4. (Color online) (a) Power spectra $P_s(f)$ of the ultrasonic echoes from the microspheres. (b) Power spectrum $P_r(f)$ of the ultrasonic echoes from the silicone plate.

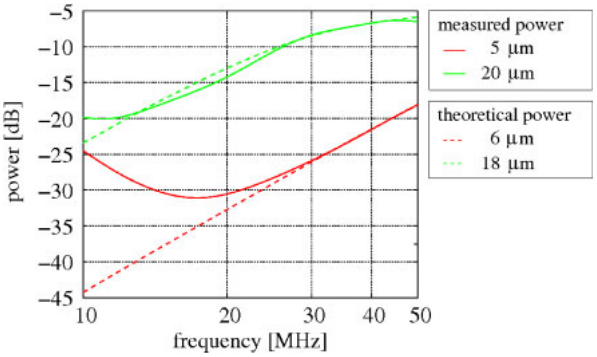

Fig. 5. (Color online) Measured normalized power spectra $\log_{10}[P_s(f)/P_r(f)]$ of microspheres, theoretical power spectra $\log_{10}[Q(ka)/4\pi a^2]$ corresponding to the estimated scatterer diameters, and weighting function $w(f_k)$.

Figure 6 shows the mean values and standard deviations of the estimated scatterer diameters of 5 and 20 µm. The mean values were 4.7 and 17.3 µm and the standard deviations were 1.9 and 1.4 µm, respectively.

3.2 In vivo measurements

The diameter of an RBC is about 8 µm. We set the lower and upper limits for the estimated scatterer sizes as 4 and 50 µm, respectively. Figure 7 shows a B-mode image of the RF echoes acquired from the posterior wall of a vein. As described in Sect. 2.3, we selected beams with echoes from a lumen–intima interface located far from the echoes from a media–adventitia interface.

Figure 8 shows a comparison among the frequency spectra of the echoes from the posterior wall of the vein. Using the

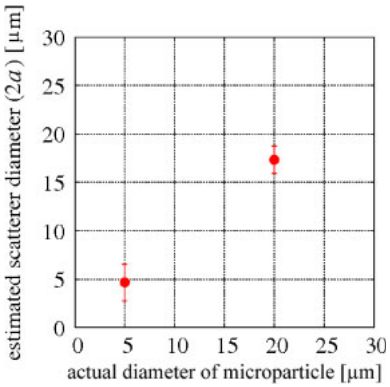

Fig. 6. (Color online) Mean values and standard deviations of the estimated scatterer diameters of 5 and 20 μm.

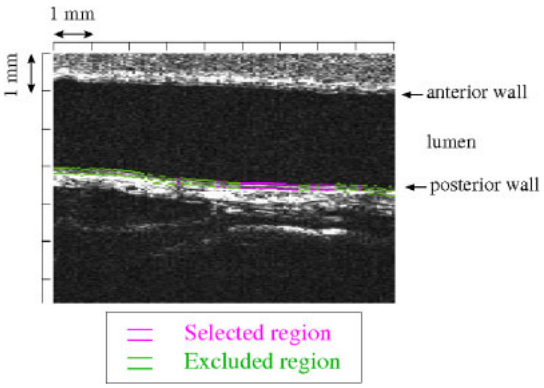

Fig. 7. (Color online) B-mode image of RF echoes from the posterior wall of a vein at the dorsum manus.

conventional process, the spectrum in Fig. 8(a) was calculated using all echoes from the posterior wall of the vein, as expressed by

$$\mathop{\mathrm{E}}_{\forall \text{beams}} \lfloor |\mathrm{F}[y(t)]|^2 \rfloor, \tag{6}$$

where F denotes the Fourier transform and $[y(t)]$ denotes RF echoes from the posterior wall of the vein. When multiple broad-band echoes return from different depths, dips appear in the frequency spectrum of the received signal at the frequency determined by the interference between echoes. The conventional process extracted the echo from the lumen–intima interface, which is overlaid by the echo from the media–adventitia interface, resulting in the appearance of a dip at 25 MHz in the frequency spectrum.

Figure 8(b) shows the spectrum obtained using the selected echoes from the lumen–intima interface, as expressed by

$$\mathop{\mathrm{E}}_{\text{well separated beams}} \lfloor |\mathrm{F}[y(t)]|^2 \rfloor. \tag{7}$$

Figure 8(c) shows a comparison of the reference spectra obtained by incoherent integration and coherent integration. The red spectrum in Fig. 8(c) is the same as the average spectrum in Fig. 8(b). The blue spectrum in Fig. 8(c) was obtained by the coherent integration process, as expressed by

$$\left| \mathop{\mathrm{E}}_{\text{beam } i \in \{\text{well separated beams}\}} [\mathrm{F}[y(t-\tau_i)]] \right|^2, \tag{8}$$

where τ_i is the time shift determined for the ith beam number.

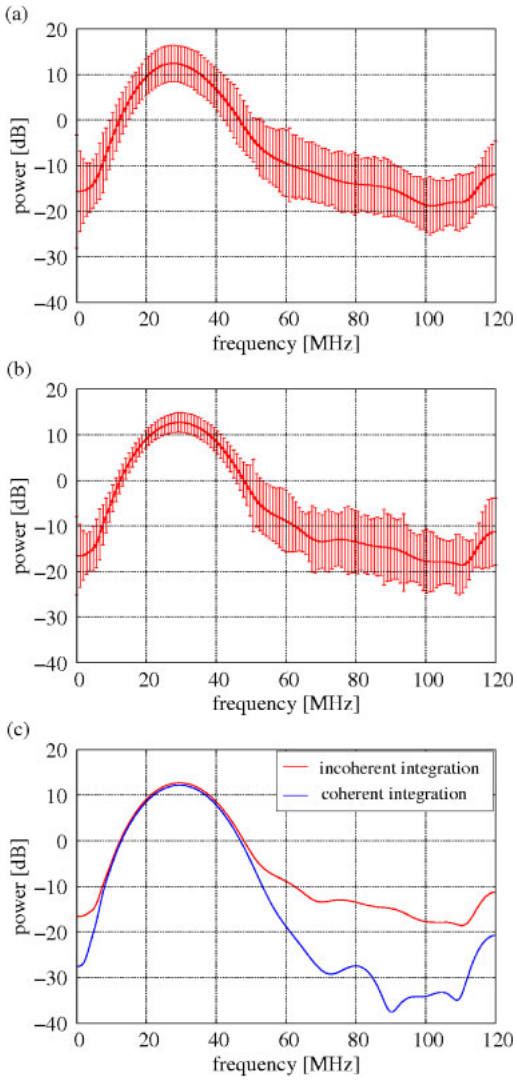

Fig. 8. (Color online) Averaged power spectrum for the reference echo, where each error bar shows the standard deviation. (a) Conventional reference power spectrum $P_r(f)$ averaged among all beams. (b) Reference power spectrum $P_r(f)$ averaged among the selected beams. (c) Comparison of the reference power spectra $P_r(f)$ calculated by incoherent integration and coherent integration after beam selection.

Figures 9 and 10 show the B-mode images of the dorsum vein of a 23-year-old healthy subject (subject A) and those of a diabetic patient (subject G), respectively. In the diabetic patient, the echo intensity in the lumen at rest [Fig. 10(a)] is higher than that in the healthy subject at rest [Fig. 9(a)], and almost the same as that of the healthy subject during avascularization [Fig. 9(b)].

Figures 11(a) and 11(b) respectively show the frequency spectra of the echoes from RBCs in the three healthy subjects (healthy A, B, C) and the four diabetic patients (patients D, E, F, G) that received both antithrombotic therapy and insulin therapy. The echo intensity of the RBCs increases upon avascularization using a cuff. This result shows that RBC aggregation resulted from avascularization. Table I shows the difference in the power at the center frequency from 10 and 60 MHz. The difference is significantly different between the healthy subjects and diabetic patients.

Figure 12 shows the power spectra of the echoes from the lumen–intima interface for each subject. In the present study, we improved the method of calculating reference power

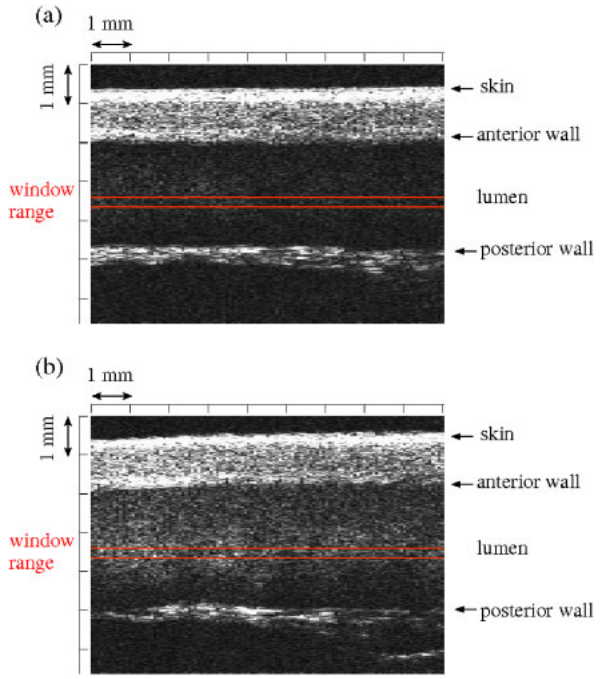

Fig. 9. (Color online) Healthy subject's B-mode images of RF echoes from the lumen during (a) rest and (b) avascularization.

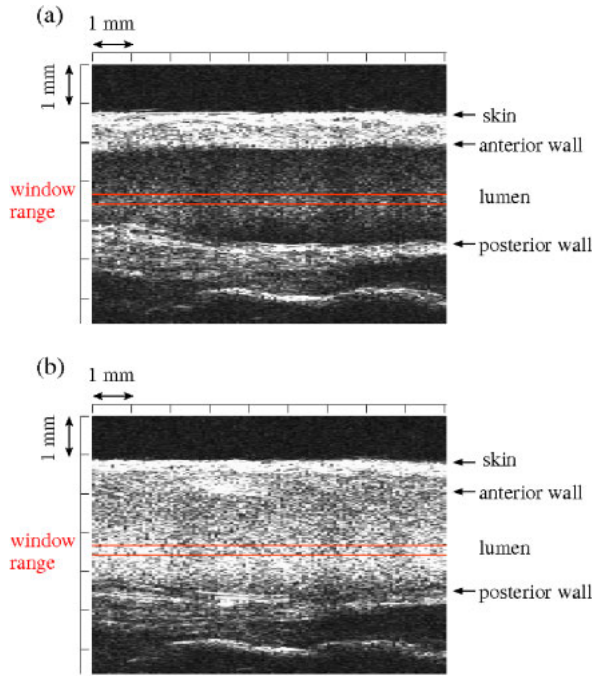

Fig. 10. (Color online) Diabetic patient's B-mode images of RF echoes from the lumen during (a) rest and (b) avascularization.

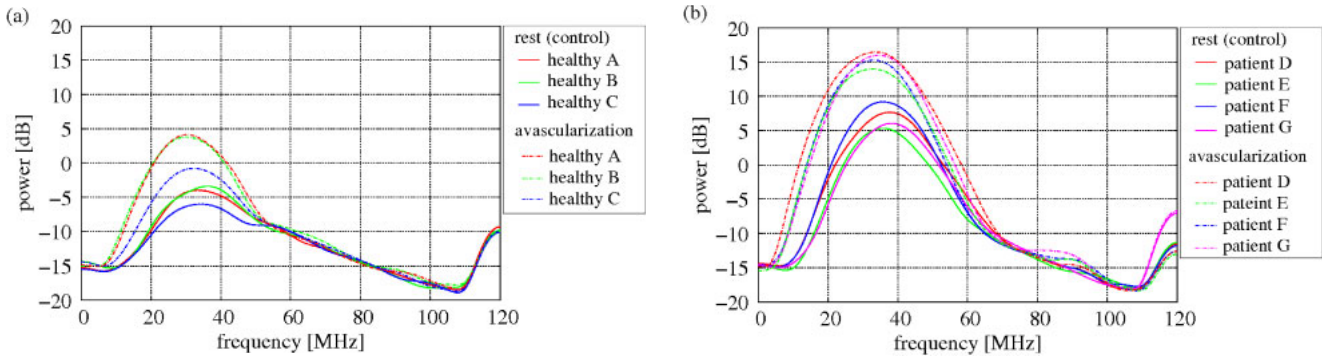

Fig. 11. (Color online) Power spectra of the echoes from RBCs for (a) healthy subjects (healthy A, B, C) and (b) diabetic patients (patients D, E, F, G).

Table I. Difference in the power of the power spectrum $P_s(f)$ at the center frequency for each subject.

Subject	From 10 MHz at rest (dB)	From 60 MHz at rest (dB)	From 10 MHz during avascularization (dB)	From 60 MHz during avascularization (dB)
Healthy A	11.2	6.6	17.3	14.3
Healthy B	11.8	7.0	16.0	13.0
Healthy C	9.4	4.0	13.2	9.2
Patient D	21.8	12.8	19.3	18.0
Patient E	19.8	13.0	20.0	19.9
Patient F	23.1	16.2	21.7	21.8
Patient G	20.6	12.5	23.1	20.5

spectra. As a result, dips in the power spectra were successfully excluded in all subjects as shown in Fig. 12.

Figure 13 shows the measured normalized power spectra and the theoretical power spectra for the estimated scatterer diameters for healthy subject A. Figures 14 and 15 show the transient changes in the estimated scatterer diameters for the three healthy subjects (healthy A, B, C) and the four diabetic patients (patients D, E, F, G), respectively. Since each diabetic patient was measured once owing to ethical considerations, Fig. 15 has no error bars. In the healthy subjects, the scatterer diameters at rest ranged from 4 to 12 μm, close to that of non-aggregated RBCs. On the other hand, the scatterer diameters during avascularization were larger than those at rest, showing that the proposed method succeeded in estimating the RBC aggregation originating from avascularization. The averages of the estimated scatterer

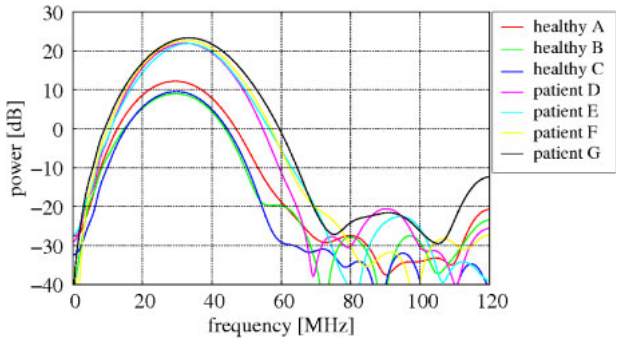

Fig. 12. (Color online) Power spectra $P_r(f)$ of the echoes from the posterior wall of the vein of the seven subjects.

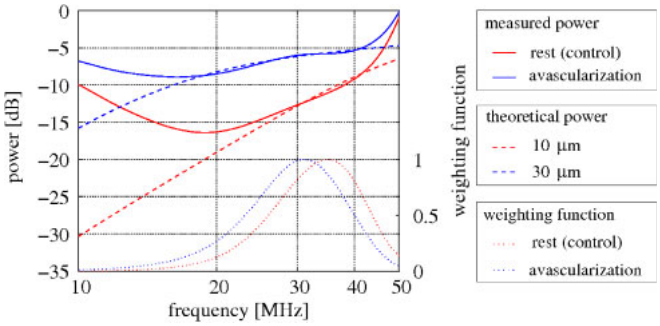

Fig. 13. (Color online) Normalized power spectra $\log_{10}[P_s(f)/P_r(f)]$, theoretical power spectra $\log_{10}[Q(ka)/4\pi a^2]$ corresponding to the estimated scatterer diameters, and weighting functions $w(f_k)$.

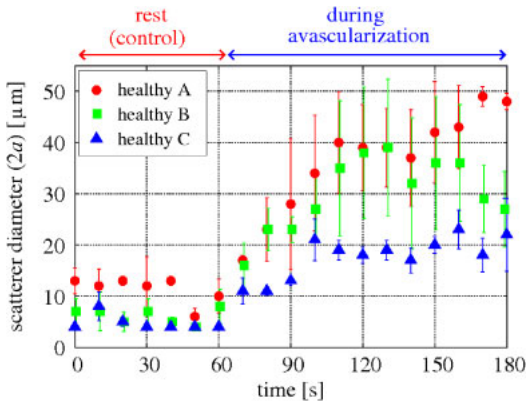

Fig. 14. (Color online) Transient changes in average estimated scatterer diameters with standard deviations during a 3 min period obtained by three in vivo measurements of three healthy subjects.

diameters in the healthy subjects at rest (0 to 60 s) and during avascularization (70 to 180 s) were 7 and 28 μm, respectively. In contrast, those in the diabetic patients receiving both antithrombotic therapy and insulin therapy were 11 and 46 μm, respectively.

Figure 16 shows the average scatterer diameter of 26 diabetic patients (a) at rest and (b) during avascularization estimated by the proposed method plotted against HbA1c, an indicator used in diabetic control. A diabetes specialist graded the 26 patients from 1 (mild) to 3 (severe) according to the severity of their diabetes based on vascular complications resulting from diabetes. We eliminated three patients with type I diabetes and two inpatients with type II diabetes from the 26 patients, and classified the remaining 21

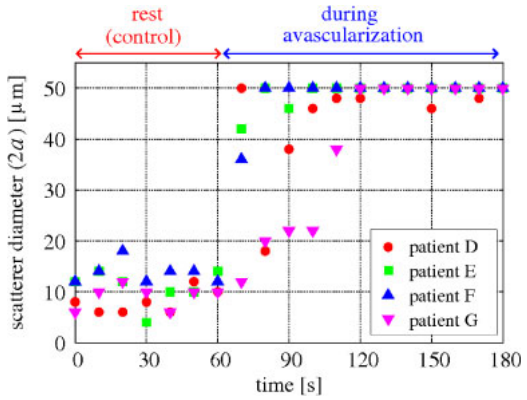

Fig. 15. (Color online) Transient changes in average estimate scatterer diameters during a 3 min period for four diabetic patients.

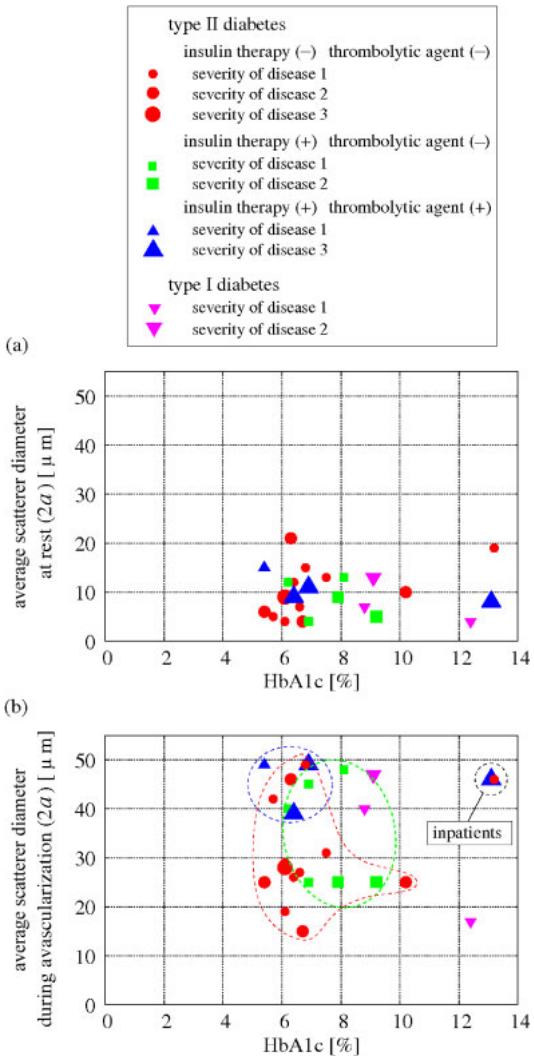

Fig. 16. (Color online) Average scatterer diameter of 26 diabetic patients (a) at rest and (b) during avascularization estimated by the proposed method plotted against HbA1c, an indicator used in diabetic control.

patients into three groups: patients without any antithrombotic therapy or insulin therapy (red), patients receiving insulin therapy only (green), and patients receiving both antithrombotic therapy and insulin therapy (blue). The blue group is considered to comprise patients with the most severe diabetes. During avascularization, the estimated scatterer diameter of the group receiving both antithrombotic therapy

and insulin therapy (blue) was larger than those of the other two groups as shown in Fig. 16(b). This finding shows that RBC aggregation depends on the severity of diabetes.

4. Conclusions

We have herein proposed a method by which the degree of red blood cell (RBC) aggregation can be assessed using the scattering property of RBCs. In basic experiments in vitro, the sizes of microspheres 5 and 20 μm in diameter were estimated to be 4.7 and 17.3 μm, respectively, by the proposed method. In in vivo measurements, RF echoes from RBCs at the dorsum manus of healthy subjects and diabetic patients were measured. The measurement was performed while the subject was at rest for 1 min and during avascularization for 2 min, and the estimated scatterer diameters during avascularization were larger than those at rest. The estimated scatterer diameters of diabetic patients at rest did not always differ from those of healthy subjects, which suggests that we should reconsider the theoretical model and the evaluation method. However, during avascularization, the average scatterer diameter of healthy subjects and that of diabetic patients receiving both antithrombotic therapy and insulin therapy were 28 and 46 μm, respectively. This finding shows that RBC aggregation depends on the severity of diabetes. The power spectra of the echoes from RBCs were different between healthy subjects and diabetic patients, showing that the estimation accuracy in RBC aggregation can be improved by taking into account the intensity of the power spectrum in the future. These results show the high potential of this novel diagnostic technique for estimating RBC aggregation in cardiovascular diseases using high-frequency ultrasound.

Acknowledgment

This work was partly supported by MEXT/JSPS KAKENHI Grant Number 26630178.

1) M. Sato, H. Hasegawa, and H. Kanai, Jpn. J. Appl. Phys. **53**, 07KF03 (2014).
2) K. Tachi, H. Hasegawa, and H. Kanai, Jpn. J. Appl. Phys. **53**, 07KF17 (2014).
3) Y. Nagai, H. Hasegawa, and H. Kanai, Jpn. J. Appl. Phys. **53**, 07KF19 (2014).
4) Y. Miyachi, H. Hasegawa, and H. Kanai, Jpn. J. Appl. Phys. **54**, 07HF18 (2015).
5) R. Nagaoka, R. Iwasaki, M. Arakawa, K. Kobayashi, S. Yoshizawa, S. Umemura, and Y. Saijo, Jpn. J. Appl. Phys. **54**, 07HF08 (2015).
6) S. Sasaki, R. Takagi, K. Matsuura, S. Yoshizawa, and S. Umemura, Jpn. J. Appl. Phys. **53**, 07KF10 (2014).
7) H. Sasaki, J. Yasuda, R. Takagi, T. Miyashita, K. Goto, S. Yoshizawa, and S. Umemura, Jpn. J. Appl. Phys. **53**, 07KF11 (2014).
8) J. Yasuda, T. Miyashita, K. Taguchi, S. Yoshizawa, and S. Umemura, Jpn. J. Appl. Phys. **54**, 07HF21 (2015).
9) D. G. Paeng, R. Y. Chiao, and K. K. Shung, Ultrasound Med. Biol. **30**, 815 (2004).
10) N. Saitoh, H. Hasegawa, and H. Kanai, Jpn. J. Appl. Phys. **48**, 07GJ08 (2009).
11) T. Yoshida, K. Sato, and T. Kondo, Jpn. J. Appl. Phys. **53**, 07KF01 (2014).
12) H. Takahashi, H. Hasegawa, and H. Kanai, Jpn. J. Appl. Phys. **53**, 07KF08 (2014).
13) C. C. Huang and S. H. Wang, Jpn. J. Appl. Phys. **45**, 7191 (2006).
14) J. J. Bishop, P. R. Nance, A. S. Popel, M. Intaglietta, and P. C. Johnson, Am. J. Physiol. Heart Circ. Physiol. **286**, H113 (2004).
15) B. Chong-Martinez, T. A. Buchanan, R. B. Wenby, and H. J. Meiselman, Diabetic Med. **20**, 301 (2003).
16) Q. Li, L. Li, and Y. Li, J. Clin. Lab. Anal. **29**, 387 (2015).
17) H. Schmid-Schönbein and E. Volger, Diabetes **25**, 897 (1976).
18) S. M. Razavian, V. Atger, P. Giral, M. Cambillau, M. Del-Pino, A. C. Simon, N. Moatti, and J. Levenson, Arterioscler. Thromb. Vasc. Biol. **14**, 361 (1994).
19) X. Wang, L. Liu, T. O. Cheng, Z. Li, Y. Deng, and J. Wang, Am. Heart J. **124**, 961 (1992).
20) T. Sato, H. Tojo, and Y. Watanabe, Jpn. J. Appl. Phys. **52**, 07HF18 (2013).
21) D. G. Paeng, K. H. Nam, and K. K. Shung, Ultrasound Med. Biol. **36**, 1118 (2010).
22) D.-G. Paeng, K.-H. Nam, M. J. Choi, and K. K. Shung, IEEE Trans. Ultrason. Ferroelectr. Freq. Control **56**, 880 (2009).
23) R. Libgot-Callé, F. Ossant, Y. Gruel, P. Lermusiaux, and F. Patat, Ultrasound Med. Biol. **34**, 252 (2008).
24) R. Callé, C. Plag, F. Patat, and F. Ossant, J. Acoust. Soc. Am. **125**, 530 (2009).
25) E. Franceschini, F. T. H. Yu, F. Destrempes, and G. Cloutier, J. Acoust. Soc. Am. **127**, 1104 (2010).
26) T. Fukushima, H. Hasegawa, and H. Kanai, Jpn. J. Appl. Phys. **50**, 07HF02 (2011).
27) I. Fontaine and G. Cloutier, J. Acoust. Soc. Am. **113**, 2893 (2003).
28) P. M. Morse and H. Feshbach, *Methods of Theoretical Physics* (McGraw-Hill, New York, 1953).
29) J. Dusting, E. Kaliviotis, S. Balabani, and M. Yianneskis, J. Biomech. **42**, 1438 (2009).
30) D. Xu, E. Kaliviotis, A. Munzjiza, E. Avital, and C. Ji, J. Biomech. **46**, 1810 (2013).